Quasi-Two-Dimensional Anomalous Hall Mott Insulator of Topologically Engineered $J_{\mathrm{eff}} = 1/2$ Electrons

Junyi Yang,[1] Hidemaro Suwa,[2] Derek Meyers,[3,4] Han Zhang,[1] Lukas Horak,[5] Zhaosheng Wang,[6] Gilberto Fabbris,[7] Yongseong Choi,[7] Jenia Karapetrova,[7] Jong-Woo Kim,[7] Daniel Haskel,[7] Philip J. Ryan,[7,8] M. P. M. Dean,[3] Lin Hao,[6,*] and Jian Liu[1,†]

[1]*Department of Physics and Astronomy, University of Tennessee, Knoxville, Tennessee 37996, USA*
[2]*Department of Physics, University of Tokyo, Tokyo 113-8656, Japan*
[3]*Department of Condensed Matter Physics and Materials Science, Brookhaven National Laboratory, Upton, New York 11973, USA*
[4]*Department of Physics, Oklahoma State University, Stillwater, Oklahoma 74078, USA*
[5]*Department of Condensed Matter Physics, Charles University, Ke Karlovu 5, 12116 Prague, Czech Republic*
[6]*Anhui Key Laboratory of Condensed Matter Physics at Extreme Conditions, High Magnetic Field Laboratory, HFIPS, Chinese Academy of Sciences, Hefei, Anhui 230031, China*
[7]*Advanced Photon Source, Argonne National Laboratory, Argonne, Illinois 60439, USA*
[8]*School of Physical Sciences, Dublin City University, Dublin 9, Ireland*

(Received 9 November 2021; revised 25 April 2022; accepted 2 June 2022; published 22 July 2022)

We investigate an experimental toy-model system of a pseudospin-half square-lattice Hubbard Hamiltonian in $[(SrIrO_3)_1/(CaTiO_3)_1]$ to include both nontrivial complex hopping and moderate electron correlation. While the former induces electronic Berry phases as anticipated from the weak-coupling limit, the latter stabilizes an antiferromagnetic Mott insulator ground state analogous to the strong-coupling limit. Their combined results in the real system are found to be an anomalous Hall effect with a nonmonotonic temperature dependence due to the competition of the antiferromagnetic order and charge excitations in the Mott state, and an exceptionally large Ising anisotropy that is captured as a giant magnon gap beyond the superexchange approach. The unusual phenomena highlight the rich interplay of electronic topology and electron correlation in the intermediate-coupling regime that is largely unexplored and challenging in theoretical modeling.

DOI: 10.1103/PhysRevX.12.031015

Subject Areas: Condensed Matter Physics
Strongly Correlated Materials

I. INTRODUCTION

The concept of topology has revolutionized the understanding of quantum materials. Successful developments have been made within the past decade in describing and discovering a variety of novel topological phases, symmetry-protected states, and Hall effects in noninteracting electronic systems [1–6]. Electron correlation, on the other hand, remains a profound and challenging problem, where rich and fascinating emergent phenomena have been known or predicted for a long time and are yet to be fully understood, such as Mott transition, unconventional superconductivity, and quantum magnetism [7–13]. Fundamental interest arises in systems where both electron correlation and electronic topology play significant roles [14–20]. Their interplay in this extensive and largely unexplored regime could provide not only new routes to unresolved problems but also opportunities for stabilizing novel quantum states [21,22].

A key quantity in electronic topology is the Berry phase, which can be expressed as the gauge-invariant phase change of the wave function acquired when a particle circles around a closed loop [4]. This phase change can be conceptualized as a fictitious magnetic field applied to a moving charge carrier, giving rise to an anomalous velocity in transport, such as that causing the anomalous Hall effect (AHE) [5]. In single-particle band structures, the Berry phase often concentrates near band crossing, such as Dirac points, in the momentum space. Many microscopic models encode these effects using complex hopping parameters,

*To whom correspondence should be addressed. haolin@hmfl.ac.cn

†To whom correspondence should be addressed. jianliu@utk.edu

with famous examples being the Haldane model [23] and the Kane-Mele model [24,25] for two-dimensional (2D) topological band insulators on honeycomb lattices. In Mott materials, however, electrons are localized in real space and charge hopping is considered as a perturbation that gives rise to superexchange interactions [26]. The incompatibility between these two opposite views of the electronic structure highlights the challenge in understanding topological correlated systems [12,14]. Although the magnetic orders of correlated electrons have been exploited as time-reversal symmetry-breaking fields for lifting topological bands and Dirac points [27], this mean-field approach remains an effective single-particle method and could fail to predict or account for many-body effects.

An alternative strategy is to experimentally realize toy-model materials, where the topology-correlation interplay can be captured and controlled by engineering the complex hopping as well as the correlation strength. The design of such systems thus necessarily requires strong spin-orbit coupling (SOC), which is the source of complex hopping [4]. A proper symmetry configuration is also essential since strong SOC itself does not guarantee nontrivial topology. Meanwhile, the correlation strength should be in the intermediate-coupling regime, which connects the opposite limits and provides the reconciliation of the two incompatible views. This regime is also the more interesting and yet challenging regime for theoretical descriptions due to the proximity to the Mott transition [7,28–32] and spatial charge-spin fluctuations [7,14,32,33]. To fulfill these requirements, we designed and realized an artificial layered iridate $[(SrIrO_3)_1/(CaTiO_3)_1]$ to simulate a single-orbital square-lattice Hubbard Hamiltonian in the intermediate-coupling regime where SU(2) symmetry-breaking complex hopping is implemented by symmetry engineering and the strong SOC of the $5d$ electrons.

II. RESULTS

A. Implementing spin-dependent hopping via artificial synthesis

The single-orbital square-lattice Hubbard Hamiltonian is an iconic model of correlated physics with the $S = 1/2$ CuO_2 plane being one of the most profound examples [8,34]. While SOC is small for Cu, it has been recently recognized that a partially analogous system can be achieved with the $J_{\mathrm{eff}} = 1/2$ state of Ir^{4+} ion on a IrO_2 plane [35–40]. A key difference is that, due to the spin-orbit-entangled $J_{\mathrm{eff}} = 1/2$ wave function [37,41], significant spin-dependent hopping arises when breaking the local inversion symmetry [42–45]. The effective Hubbard Hamiltonian can be written as [42–46]

$$H = -t\sum_{\langle ij\rangle}\sum_{\alpha,\beta}[c^{\dagger}_{i\alpha}(e^{i\theta \boldsymbol{d}_{ij}\cdot\boldsymbol{\sigma}})_{\alpha\beta}c_{j\beta} + \mathrm{H.c.}] + U\sum_i n_{i\uparrow}n_{i\downarrow}, \quad (1)$$

where the first term accounts for the nearest-neighboring $\langle ij\rangle$ hopping, $c^{\dagger}_{i\alpha}$ ($c_{i\alpha}$) is the creation (annihilation) operator of a $J_{\mathrm{eff}} = 1/2$ electron with spin α on site i, $\boldsymbol{\sigma}$ is the vector of Pauli matrices, and U is the onsite electron-electron repulsion. The parameter θ in the SU(2) gauge field $e^{i\theta \boldsymbol{d}_{ij}\cdot\boldsymbol{\sigma}}$ [47] controls the imaginary (spin-dependent) and real (spin-independent) hopping of a Ir—O—Ir bond by the ratio $\tan\theta$, whereas the unit vector $\boldsymbol{d}_{ij}$ depends on oxygen displacement of the bond [46]. θ thus characterizes the size of the displacement and depends on the bond angle [46,48].

The IrO_6 octahedral layer is an ideal building block for simulating such a Hubbard Hamiltonian not only because large θ can be afforded by the SOC but also due to the intermediate-U/t value of $5d$ electrons [30,33,49,50]. Previous studies have explored the situation where the spin-dependent hopping preserves the continuous spin rotational symmetry [33,43], i.e., a SU(2) symmetry which is *hidden* but can be revealed when the spin-dependent hopping of all bonds is removed simultaneously by a gauge transformation [46]. The interesting open question is what would happen if the hidden SU(2) symmetry is broken. The key to realizing such a toy-model material is the control of the lattice symmetry, which we achieved by growing $[(SrIrO_3)_1/(CaTiO_3)_1]$ superlattices (SLs) [Fig. 1(a)] with 30 repeats on (001)-oriented $SrTiO_3$ single-crystal substrates by pulsed laser deposition (see Sec. III). This design implements significant octahedral tilt around the two in-plane axes and lowers the symmetry, which is inspired by the idea of reducing the effective tolerance factor of the reported rotation-only $[(SrIrO_3)_1/(SrTiO_3)_1]$ SL [51,52], by replacing the confining $SrTiO_3$ monolayers with $CaTiO_3$. We defined the reciprocal lattice based on an $a \times a \times 2c$ supercell, where $a = 3.905$ Å and $c = 3.892$ Å are the pseudo-cubic in-plane and out-of-plane lattice parameters, respectively, extracted from x-ray diffraction (XRD). Figure 1(b) shows the primary (0 0 even) film peaks, which almost overlap with the substrate peaks, as well as the (0 0 3) satellite reflection that confirms the layered structure [Fig. 1(a)]. Thus, while each IrO_6 octahedral layer can be effectively described by the minimal 2D model in Eq. (1), a small but nonzero interlayer coupling exists to stabilize any long-range magnetic order [52]. A fully strained state was also confirmed by reciprocal space mapping, shown in Supplemental Material, Fig. S1 [53]. The octahedral pattern was verified by measuring a set of half-order peaks. For instance, the (0.5 1.5 3) peak [Fig. 1(d)] representing octahedral rotation is observed, shown also in Supplemental Material, Fig. S3 [53]. Shown in Fig. 1(c) is a pronounced (0.5 0.5 3) reflection that is characteristic of a significant octahedral tilt [54].

B. Mott state of intermediate coupling regime

We first established the electronic ground state of the SL as a Mott insulator by measuring the longitudinal

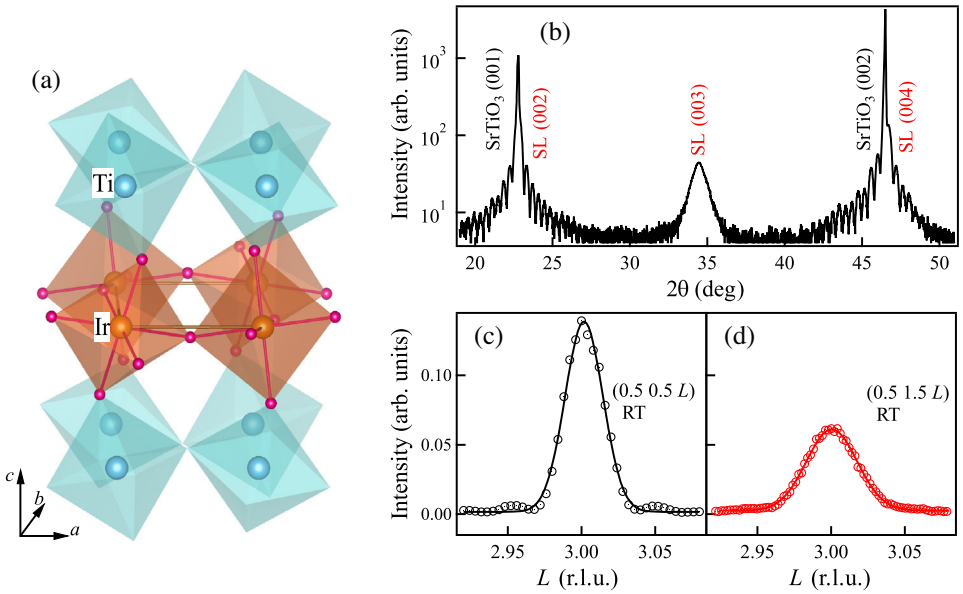

FIG. 1. Structure characterization. (a) Crystal structure of the $[(SrIrO_3)_1/(CaTiO_3)_1]$ SL grown on a $SrTiO_3$ substrate. (b) X-ray θ-2θ scan pattern of the SL. (c),(d) Room-temperature (RT) synchrotron XRD measured around the (0.5 0.5 3) and (0.5 1.5 3) peaks.

resistivity that increases with lowering temperature [Fig. 2(c)], and confirmed the square-lattice antiferromagnetic (AFM) order by probing the (0.5 0.5 integer) AFM Bragg peak with resonant x-ray magnetic scattering [Fig. 2(a)]. The AFM order in one IrO_6 octahedral layer is thus related to another simply by vertical translation. The integrated peak intensity recorded as a function of temperature reveals $T_N \sim 170$ K [Fig. 2(b)]. These results

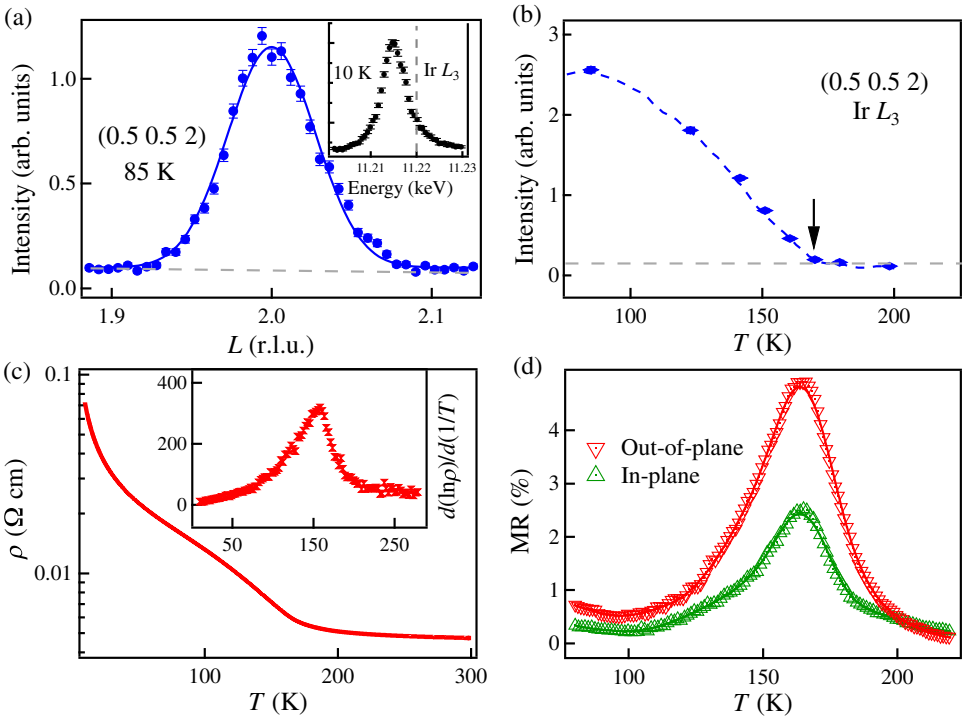

FIG. 2. Magnetic structure and magnetoresistance effect. (a) L scan across the (0.5 0.5 2) magnetic peak. Dashed line represents the background signal. Error bar represents statistical error. Inset shows the energy profile at 10 K, where a vertical dashed line indicates the Ir-L_3 absorption edge. (b) Integrated intensity of magnetic peak versus temperature. T_N is denoted by a black arrow. (c) Temperature dependence of in-plane resistivity. Inset shows the relation between $d(\ln\rho)/d(1/T)$ and temperature. (d) Temperature-dependent MR measured under an out-of-plane (red) or in-plane (green) 8 T magnetic field.

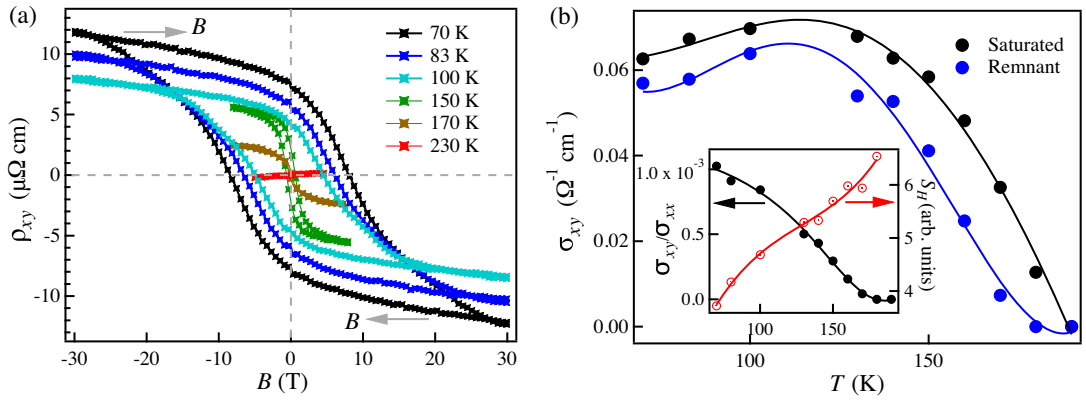

FIG. 3. Hall signatures of the topology. (a) Magnetic field dependence of Hall resistivity at different temperatures. The field sweeping directions are shown as gray arrows. (b) Temperature dependences of the saturated and remnant Hall conductivity. Inset shows the temperature dependences of σ_{xy}/σ_{xx} and S_H [53].

conclude that the correlation strength of $[(SrIrO_3)_1/(CaTiO_3)_1]$ is sufficiently large to stabilize an AFM Mott insulating state.

Figure 2(c) indicates that the wide-gap dielectric $CaTiO_3$ spacer in the $[(SrIrO_3)_1/(CaTiO_3)_1]$ SL plays virtually the same role as $SrTiO_3$ in confining the $SrIrO_3$ monolayer in the $[(SrIrO_3)_1/(SrTiO_3)_1]$ SL to form the quasi-2D SL [55], considering their similarity in both the RT resistivity and the resistivity increase when cooling to 10 K [53]. More importantly, there are clear signatures that the U/t value of $[(SrIrO_3)_1/(CaTiO_3)_1]$, similar to the $[(SrIrO_3)_1/(SrTiO_3)_1]$ SL, falls into the intermediate regime, such as a resistivity kink right below T_N [Fig. 2(c)], which implies significant charge fluctuations that are suppressed upon long-rang AFM ordering [33]. Suppressing these charge fluctuations by magnetic field results in a positive anomalous magnetoresistance (MR) with a critical enhancement in the paramagnetic insulating phase [Fig. 2(d)]. This magneto-charge transport response above T_N is due to the fact that the charge fluctuations are tied with the longitudinal AFM fluctuations and the external uniform field suppresses them by acting as an effective staggered field and inducing finite staggered magnetization. This staggered field effect is due to the gauge-dependent component of the imaginary hopping in Eq. (1) [33]. Specifically, the response to the in-plane field is attributed to the out-of-plane component of the $\boldsymbol{d}_{ij}$ vectors [56] that originates from the octahedral rotation and can be gauged away by a staggered rotation transformation around the c axis, as demonstrated in the $[(SrIrO_3)_1/(SrTiO_3)_1]$ SL [33]. The response to the out-of-plane field, on the other hand, demonstrates that the in-plane component of the $\boldsymbol{d}_{ij}$ vectors (induced by the tilt) also contributes to the gauge-dependent imaginary hopping as shown in Fig. 4(c). All in all, the significant field-tunable spin-charge fluctuations are unexpected for a strong Mott insulator but characteristic of the intermediate-coupling regime where the correlated charge gap allows excitations into the electron-hole continuum.

C. Hall signature of topology

In addition to the anomalous MR, the charge fluctuations also manifest in the emergence of a spontaneous Hall effect upon broken time-reversal symmetry in $[(SrIrO_3)_1/(CaTiO_3)_1]$. One can see a nonlinear Hall signal with the out-of-plane field developing around T_N, and it evolves into a hysteresis loop with a significant remnant Hall resistance upon cooling [Fig. 3(a)]. The necessity of significant octahedral tilting in leading to AHE is corroborated by the absence of any observable AHE on $[(SrIrO_3)_1/(SrTiO_3)_1]$ SLs with vanishing octahedral tilting [30,53]. The temperature-dependent behavior as seen in Fig. 3(b) is quite unique in that both the extracted saturated and remnant values of the AHE conductivity start to decrease with cooling after a sharp increase below T_N.

This behavior is a result of the fact that the thermally activated charge carriers and the local AFM moments come from the same group of electrons, and they necessarily increase at the expense of each other. The AHE conductivity is thus subjected to a self-competition because it relies on both the charge carriers and the time-reversal symmetry-breaking field from the AFM order. Such competition is also captured by the anomalous Hall angle σ_{xy}/σ_{xx} and the anomalous Hall conductivity coefficient $S_H = \sigma_{xy}/M_s$ [57] [see the inset of Fig. 3(b)], where M_s is the staggered magnetization. The former indicates that the current is increasingly deflected upon cooling (i.e., the magnetic order becomes stronger and stronger), while the latter suggests that the charge carriers contributing to the transverse channel drop quickly below T_N. These observations highlight the topology-correlation interplay in the intermediate coupling regime of the Hubbard Hamiltonian. In other words, the observed AHE is completely driven by the same group of electrons (i.e., the $J_{\text{eff}} = 1/2$ electrons) that form the AFM Mott insulating state, which is in sharp contrast to the AHE reported in iridate-manganite, iridate-cobaltite, and iridate-ruthenate heterostructures, where the strong spin-orbit coupled $5d$

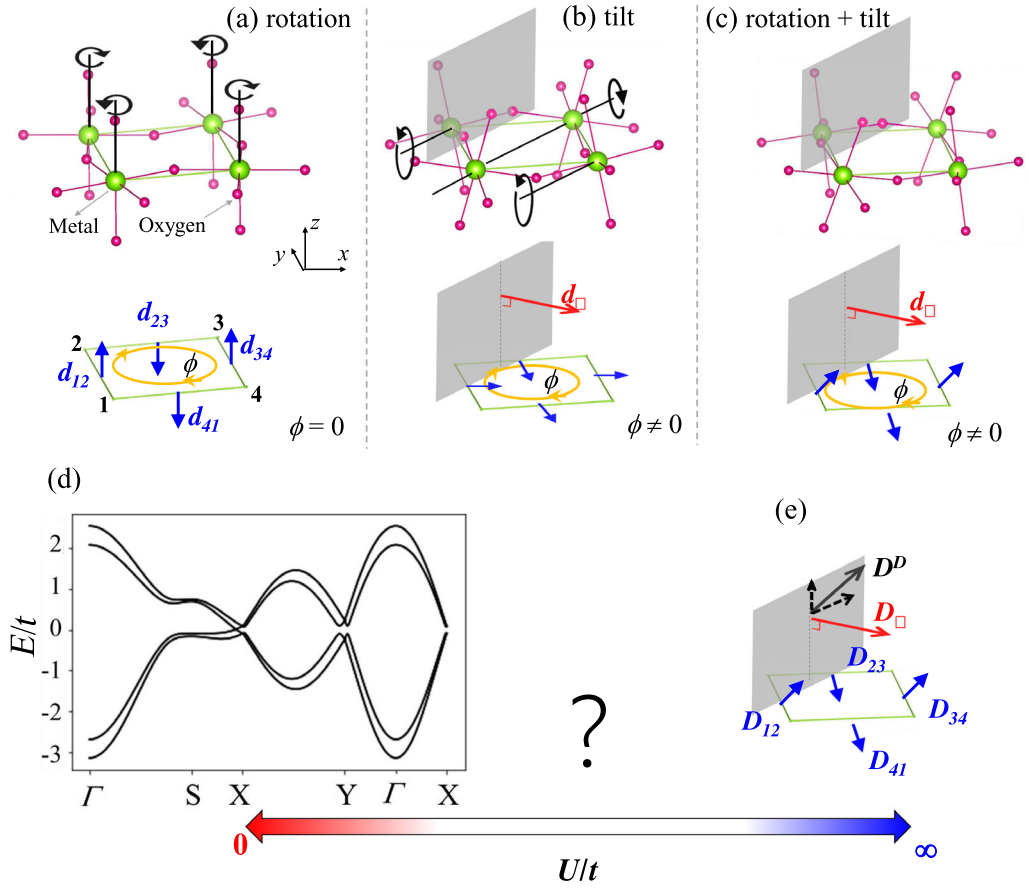

FIG. 4. Spin-dependent hopping of the Hubbard model. A perovskite square lattice with (a) octahedral rotations ($p4g$ wallpaper group containing a fourfold rotational symmetry and a glide reflection), (b) octahedral tilts (pg wallpaper group containing a glide reflection), or (c) octahedral rotations and tilts (pg wallpaper group). Bottom panels show the modulation of $\boldsymbol{d}_{ij}$ vectors (blue arrows). Octahedral rotation or tilts on neighboring sites are opposite. The finite $\boldsymbol{d}_\square$ (red arrow) in (b) and (c) is perpendicular to the mirror plane (gray) of the b-glide symmetry. (d) Representative $U = 0$ band structure for a quasi-2D structure with two layers of square lattice (c) [53]. (e) Schematic diagram of Dzyaloshinskii–Moriya (DM) interactions on the square lattice (c) at the strong-coupling limit $U = \infty$. The blank space with a question mark highlights the extensive and largely unexplored intermediate region among the two limits.

electrons and the $3d$ ($4d$) electrons play separate roles in the physical properties [58–62].

D. Discussion on square-lattice Hubbard model with broken SU(2) symmetry

The emergence of Berry phases can be captured by Eq. (1) if the spin-dependent hopping has an SU(2) symmetry-breaking component. The case of a hidden SU(2) symmetry mentioned above corresponds to a c-axis octahedral rotation-only structure, such as the $[(SrIrO_3)_1/(SrTiO_3)_1]$ SL [51,52], where $\boldsymbol{d}_{ij} = (-1)^i\hat{z}$ allows the SU(2) gauge fields of all bonds in Eq. (1) to be gauged away simultaneously by a staggered frame transformation [Fig. 4(a)] [35,43,46]. In this scenario, despite θ being finite, the gauge-invariant flux ϕ of hopping around a plaquette, i.e., the sum of the phases of the gauge field along a closed loop, is zero, the same as that when $\theta = 0$ [5]. Thus, the noninteracting band structure is an ordinary metal without finite Berry curvature, which is true even with further-neighbor hopping [43]. ϕ could become finite if the local bond-inversion symmetry breaking not only turns on θ but also breaks the hidden SU(2) symmetry [63]. As shown in Fig. 4(b), the octahedral tilt around a diagonal axis of the square plaquette removes the fourfold rotation symmetry [64]. Such a 2D lattice has a pg wallpaper group [65]. The $\boldsymbol{d}_{ij}$ vectors on the $\boldsymbol{x}$ and $\boldsymbol{y}$ bonds are no longer along the same axis but rotated by 90° from each other due to the remaining glide plane, which means that it is no longer possible to simultaneously gauge away the spin-dependent hopping of all bonds, i.e., a broken SU(2) symmetry. The finite ϕ around a plaquette, to the first order of θ in expanding $e^{i\theta \boldsymbol{d}_{ij}\cdot\sigma}$, scales with the gauge-invariant vector $\boldsymbol{d}_\square \equiv \sum_\square \boldsymbol{d}_{ij}$ (where $\square$ stands for the consecutive sum over a plaquette), which represents the SU(2) symmetry-breaking component of the spin-dependent hopping and is normal to the glide plane [Fig. 4(b)]. When both rotation and tilt are present as that

shown in the $[(SrIrO_3)_1/(CaTiO_3)_1]$ SL, the $\boldsymbol{d}_{ij}$ vectors become noncoplanar [Fig. 4(c)], but $\boldsymbol{d}_{\square}$ remains associated with the tilt and normal to the glide plane. Therefore, finite Berry curvatures can be anticipated in the noninteracting band structure. Indeed, tight-binding Hamiltonian calculations predicted such a 2D system to be a nonsymmorphic Dirac semimetal with Dirac points near the X and Y points of the unfolded Brillouin zone [45], as shown in Fig. 4(d), and further proposed a quantum anomalous Hall phase upon breaking time-reversal symmetry [45].

However, breaking time-reversal symmetry with a spontaneous magnetic order requires a finite U value in Eq. (1), which means many-body effects may be significant. Indeed, while our observation of AHE in Fig. 3 is qualitatively consistent with the presence of Berry curvatures described by the noninteracting band structure, the observed Mott insulating behavior at temperatures well above T_N in Fig. 2(c) indicates that the correlation strength of the SL is too strong for the noninteracting picture. On the other hand, in the large-U/t limit, the Hubbard model has been studied in a very different perspective, i.e., mapping Eq. (1) to a Heisenberg-like model with anisotropic superexchange interactions described by the Moriya vector $\boldsymbol{D}_{ij} = (4t^2/U)\sin 2\theta \cdot \boldsymbol{d}_{ij}$ [Fig. 4(e)] [66,67]. The SU(2) symmetry-breaking component of the spin-dependent hopping would induce an Ising anisotropy along the axis of the gauge-invariant vector $\boldsymbol{D}_{\square} \equiv \sum_{\square} \boldsymbol{D}_{ij} = (4t^2/U)\sin 2\theta \cdot \boldsymbol{d}_{\square}$ [48,66,67], while the SU(2) symmetry-preserving component is described by the gauge-dependent Dzyaloshinskii vector $\boldsymbol{D}^D \equiv \sum_j \boldsymbol{D}_{ij}$ [46,68] and can be gauged away. It is clear that the consequences of the SU(2) gauge field are very different in this picture of the strong-coupling limit [48], where the electrons are fully localized to form a strong Mott insulator [Fig. 4(e)]. The observed AHE within the Mott insulating state shows that the correlation strength of the SL is far from the large-U/t limit and the topological effect survives in the Hubbard bands under a moderate electron correlation. It is thus crucial to further determine whether the topological and magnetic effects of the SU(2) gauge field could coexist in the intermediate-coupling regime or in the vicinity of the transition.

E. Emergent Ising anisotropy

The spontaneous Hall conductivity indicates that the mirror of the glide plane symmetry must be broken by the magnetic order, which is actually consistent with the expectation in the strong-coupling limit that the AFM spin axis is along the $\boldsymbol{D}_{\square}$ vector perpendicular to the glide plane [Fig. 4(e) and inset of Fig. 5(b)] [48,66,67]. While $\boldsymbol{D}_{\square}$ originates from the gauge-invariant component of the imaginary hopping [46,68], the gauge-dependent component $\boldsymbol{D}^D$ necessarily introduces spin canting of the AFM order [48]. However, the $\boldsymbol{D}^D$ vector alone does not specify a canting direction because of the rotational invariant nature of the Dzyaloshinskii–Moriya (DM) interaction. The canting direction and angle are instead determined by $\boldsymbol{D}_{\square} \times \boldsymbol{D}^D$ [48]. Under the implemented rotation and tilt, $\boldsymbol{D}_{\square}$ and $\boldsymbol{D}^D$ are normal to each other [Fig. 4(e)], which should give rise to both in-plane and out-of-plane canted moments. Our magnetization measurement [Fig. 5(a)] indeed shows both in-plane and out-of-plane remnant magnetizations below T_N. Given this weak ferromagnetic component, the anomalous Hall coefficient $R_s \equiv \rho_{xy}/M_z$ with ρ_{xy} and M_z being the Hall resistivity and out-of-plane magnetization at zero field, respectively, can be extracted [inset of Fig. 5(a)], and it increases with decreasing temperature. Interestingly, the size of R_s at the level of 1 $m\Omega\,cm/T$ is quite large compared to other ferromagnetic oxides [69,70]. This enhancement is a combined result of the primary magnetic order parameter being AFM and the charge carriers originating from thermal excitation in a Mott insulating state.

While correctly capturing the symmetry of the magnetic structure, we found that the superexchange approach is, however, insufficient to account for the strength of the Ising anisotropy, which we evaluated through resonant inelastic x-ray scattering (RIXS) measurements at the Ir L_3 edge. The technique has been widely used to measure magnon excitations in iridates [71–75], including thin films [75] and artificial SLs [76,77]. To map the dispersion of magnetic excitations, RIXS spectra were collected at multiple $\boldsymbol{Q}$ points. Indeed, we found that the overall magnon dispersion in $[(SrIrO_3)_1/(CaTiO_3)_1]$ is similar to other single-layered iridates [53] and characteristic of a square-lattice Heisenberg antiferromagnet except near the AFM wave vector (π,π) [76,78,79]. Figure 5(c) shows the energy-loss spectra at (π,π), displaying a sharp elastic peak at 0 eV and a broad bump centering at ~0.65 eV due to the overlap of spin-orbit excitation and particle-hole continuum [76,78,79], which is similar to other iridates. From 0.05 to 0.14 eV, a prominent magnon excitation is well separated from the elastic peak. For comparison, the spectrum of $[(SrIrO_3)_1/(SrTiO_3)_1]$ at the same $\boldsymbol{Q}$ point is overlaid to highlight the difference due to the breaking of the hidden SU(2) symmetry by the implemented tilt distortion.

As shown in Fig. 5(b), the extracted dispersion from the magnon peak at (π,π) gives a giant spin gap $\Delta_m \sim 85 \pm 5$ meV. Such a strong magnetic anisotropy is also responsible for the large coercive field in the AHE measurement [Fig. 3(a)]. Given a Heisenberg $J \sim 50$ meV in most iridates [76–79], this large value of Δ_m would yield $\boldsymbol{D}_{\square} \sim 160$ meV in the linear spin wave theory, which effectively requires $U/t \sim 1$ and invalidates the superexchange approach that assumes a large-U/t limit [53]. It again points to the fact that the system is in the intermediate-coupling regime, and the giant spin gap is a nontrivial and direct result of the spatial spin fluctuations through the SU(2) symmetry-breaking hopping. A theoretical estimation of the spin gap should be done directly

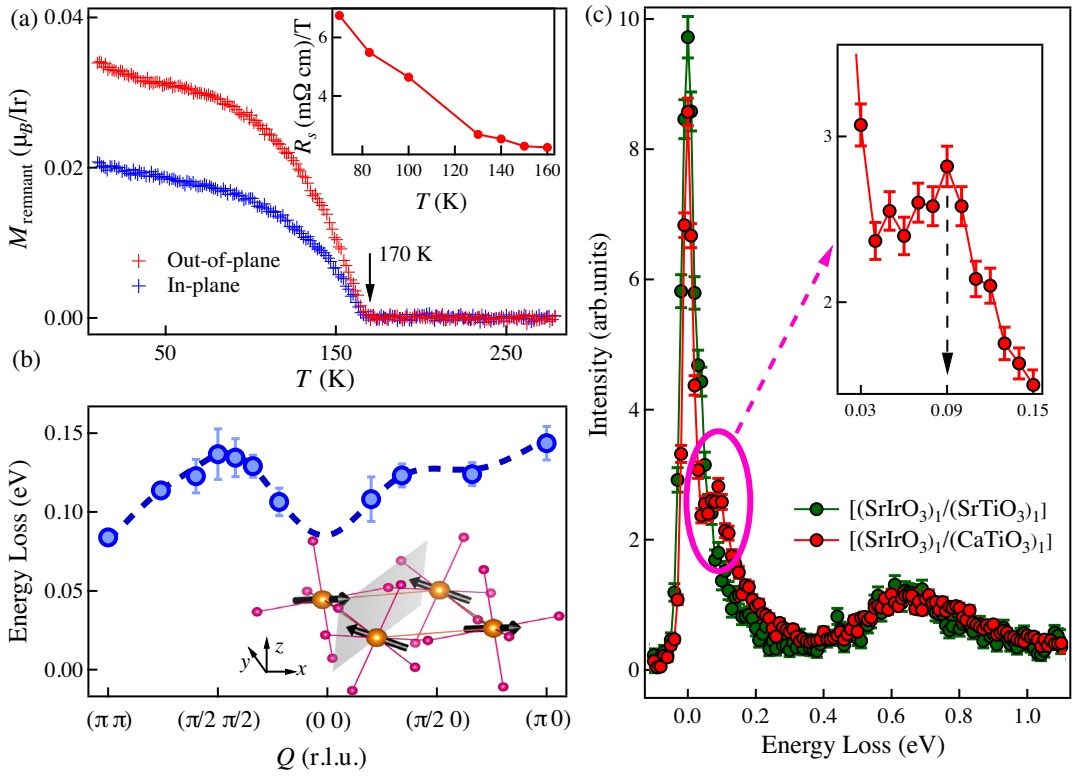

FIG. 5. Magnetic structure and low-energy magnetic excitations. (a) Temperature-dependent out-of-plane (red) and in-plane (blue) remnant magnetization (M_{remnant}). Inset shows the temperature dependence of R_s. (b) Extracted magnon peak dispersion across the Brillouin zone. The errors are statistical from the fitting with dashed line as a guide to the eye. Inset shows the ground-state magnetic pattern of the SL. The $J_{\text{eff}} = 1/2$ magnetic moments are represented as black arrows. (c) RIXS spectra at $\boldsymbol{Q} = (\pi, \pi)$ of the SL (red) and $[(SrIrO_3)_1/(SrTiO_3)_1]$ (green) measured at 35 K. The magnon excitation feature is indicated by an ellipse. Inset shows the expanded view of the magnon feature.

with the Hubbard model and indeed suggests $U/t \sim 2.5$ for such a large magnon gap [80]. A similar conclusion was recently reached in the bilayer iridate $Sr_3Ir_2O_7$ where the large spin gap should be accounted with the Hubbard model instead of an effective spin Hamiltonian due to the intermediate U/t value [81,82]. The difference is that the large spin gap there is achieved with a large bilayer interaction [83,84]. What is also different is that the c-axis collinear AFM order in $Sr_3Ir_2O_7$ preserves the point group mirror symmetry perpendicular to the ab planes [85], whereas the Ising anisotropy in the $[(SrIrO_3)_1/(CaTiO_3)_1]$ SL forces the AFM order to break the point group mirror symmetry. This difference enables AHE in the latter but not in the former since mirror symmetry of a 2D system forbids spontaneous transverse current [86].

To conclude, we have experimentally realized a quasi-2D anomalous Hall Mott insulator, which is designed to incorporate correlated and topological effects in the square-lattice Hubbard Hamiltonian with a frozen SU(2) gauge field. The results show that the gauge-dependent and gauge-invariant components of the SU(2) gauge field lead to distinct consequences that coexist in the intermediate correlation regime. In particular, the gauge-invariant component gives rise to an emergent spontaneous Hall effect, which is a signature of Berry curvatures in the electronic structure of a Mott state derived from a Dirac semimetallic phase. The electron correlation of the Mott state in turn renders the spontaneous Hall effect a nonmonotonic temperature-dependent behavior as the AFM order is necessarily stabilized at the expense of the spatial charge fluctuations that the Hall effect relies on. On the other hand, the spin axis of the AFM order is determined by the gauge-invariant component, which creates a surprisingly strong Ising anisotropy beyond the conventional superexchange approach based on the Moriya vector. The intertwining of phenomena that are usually captured in drastically different pictures of the electronic state highlights the rich and complex interplay between correlation and topology in the intermediate-coupling regime.

III. MATERIALS AND METHODS

A. Sample preparation

During the sample growth, the substrate temperature and laser fluence (KrF excimer laser beam, $\lambda = 248$ nm) were optimized to be 600 °C and 2 J/cm^2, respectively. The growth pressure was maintained to be 0.1 mbar with a constant oxygen flow. A reflection high-energy electron

diffraction unit was adopted to accurately control the stacking sequence and SL thickness (30 SL unit cells).

B. Experimental methods

The crystalline quality and lattice structure of the obtained SL were characterized on a Panalytical X'Pert MRD diffractometer. Electric transport measurements were carried out on a physical properties measurement system (Quantum Design). High-field (30 T) Hall measurement was performed on the Steady High Magnetic Field Facilities, High Magnetic Field Laboratory, Chinese Academy of Sciences. Measurements of magnetization were performed on a vibrating sample magnetometer (Quantum Design). Synchrotron x-ray diffraction experiments were performed at the 33BM beam line in the Advanced Photon Source (APS) of Argonne National Laboratory. X-ray absorption measurements were performed at the 4IDD beam line, APS. The magnetic resonant x-ray scattering experiment was carried out at the 6IDB beam line, APS. A polarization analyzer was utilized to increase the signal-to-noise ratio. The reciprocal lattice notation is defined based on a $a \times a \times 2c$ superlattice cell, where a and c are the pseudo-cubic in-plane and out-of-plane lattice parameters, respectively. The interlayer coherence length can be extracted to be $\sim 64c$ from Fig. 2(a), indicating that the quasi-2D ordering spans over the entire SL. RIXS experiments were conducted at the 27IDB beam line, APS, with a grazing incidence geometry. The reciprocal space resolution is ~ 0.12 Å^{-1} with a mask used.

ACKNOWLEDGMENTS

The authors acknowledge experimental assistance from H. D. Zhou and M. Koehler. The authors also appreciate helpful discussions with R. Zhang, C. D. Batista, E. Dagotto, S. S. Zhang, Z. T. Wang, and D. Gong. J. L. acknowledges support from the National Science Foundation under Grant No. DMR-1848269 and the Office of Naval Research (Grant No. N00014-20-1-2809). Partial funding for open access to this research was provided by University of Tennessee's Open Publishing Support Fund. H. S. acknowledges Inamori Research Grants from Inamori Foundation and support from JSPS KAKENHI Grants No. JP19K14650 and No. JP22K03508. L. Hao acknowledges support from the National Natural Science Foundation of China (Grant No. 12104460) and the High Magnetic Field Laboratory of Anhui Province (Grant No. AHHM-FX-2021-03). J. Y. acknowledges funding from the State of Tennessee and Tennessee Higher Education Commission (THEC) through their support of the Center for Materials Processing. L. Horak acknowledges support by the ERDF (Project No. CZ.02.1.01/0.0/0.0/15_003/0000485) and the Grant Agency of the Czech Republic grant (14-37427 G). Work at Brookhaven National Laboratory was supported by the U.S. Department of Energy, Office of Science, Office of Basic Energy Sciences, under Contract No. DE-SC0012704. Use of the Advanced Photon Source, an Office of Science User Facility operated for the U.S. DOE, OS by Argonne National Laboratory, was supported by the U.S. DOE under Contract No. DE-AC02-06CH11357. Part of characterization in this research was conducted at the Center for Nanophase Materials Sciences, which is a U.S. DOE Office of Science User Facility. A portion of this work was performed on the Steady High Magnetic Field Facilities, High Magnetic Field Laboratory, Chinese Academy of Sciences, and supported by the High Magnetic Field Laboratory of Anhui Province.

The authors declare that they have no competing interests.

J. L. and L. Hao conceived and directed the study. L. Hao and J. Y. undertook sample growth and characterization. L. Hao, J. Y., L. Horak, and J. K. performed structure characterization. L. Hao and Z. W. performed high-field transport measurement. L. Hao, J. Y., D. M., J. W.K and P. J. R. performed magnetic scattering measurements. L. Hao, J. Y., G. F., Y. C., and D. H. conducted XAS measurements. D. M. and M. P. M. D. performed RIXS measurements. H. S. performed the theoretical simulation. L. Hao and J. L. analyzed data. L. Hao and J. L. wrote the manuscript.

[1] Y. Ando, *Topological Insulator Materials*, J. Phys. Soc. Jpn. **82**, 102001 (2013).
[2] M. Z. Hasan and C. L. Kane, *Colloquium: Topological Insulators*, Rev. Mod. Phys. **82**, 3045 (2010).
[3] X. Wan, A. M. Turner, A. Vishwanath, and S. Y. Savrasov, *Topological Semimetal and Fermi-Arc Surface States in the Electronic Structure of Pyrochlore Iridates*, Phys. Rev. B **83**, 205101 (2011).
[4] D. Xiao, M.-C. Chang, and Q. Niu, *Berry Phase Effects on Electronic Properties*, Rev. Mod. Phys. **82**, 1959 (2010).
[5] N. Nagaosa, J. Sinova, S. Onoda, A. H. MacDonald, and N. P. Ong, *Anomalous Hall Effect*, Rev. Mod. Phys. **82**, 1539 (2010).
[6] T. Zhang, Y. Jiang, Z. Song, H. Huang, Y. He, Z. Fang, H. Weng, and C. Fang, *Catalogue of Topological Electronic Materials*, Nature (London) **566**, 475 (2019).
[7] B. H. Brandow, *Electronic Structure of Mott Insulators*, Adv. Phys. **26**, 651 (1977).
[8] E. Dagotto, *Correlated Electrons in High-Temperature Superconductors*, Rev. Mod. Phys. **66**, 763 (1994).
[9] S. Sachdev, *Quantum Magnetism and Criticality*, Nat. Phys. **4**, 173 (2008).
[10] M. Imada, A. Fujimori, and Y. Tokura, *Metal-Insulator Transitions*, Rev. Mod. Phys. **70**, 1039 (1998).
[11] D. N. Basov, R. D. Averitt, and D. Hsieh, *Towards Properties on Demand in Quantum Materials*, Nat. Mater. **16**, 1077 (2017).
[12] B. Keimer and J. E. Moore, *The Physics of Quantum Materials*, Nat. Phys. **13**, 1045 (2017).

[13] Y. Zhou, K. Kanoda, and T.-K. Ng, *Quantum Spin Liquid States*, Rev. Mod. Phys. **89**, 025003 (2017).

[14] D. Pesin and L. Balents, *Mott Physics and Band Topology in Materials with Strong Spin–Orbit Interaction*, Nat. Phys. **6**, 376 (2010).

[15] W. Qin, L. Li, and Z. Zhang, *Chiral Topological Superconductivity Arising from the Interplay of Geometric Phase and Electron Correlation*, Nat. Phys. **15**, 796 (2019).

[16] M. Hohenadler and F. F. Assaad, *Correlation Effects in Two-Dimensional Topological Insulators*, J. Phys. Condens. Matter **25**, 143201 (2013).

[17] M. J. Park, G. Sim, M. Y. Jeong, A. Mishra, M. J. Han, and S. Lee, *Pressure-Induced Topological Superconductivity in the Spin–Orbit Mott Insulator* $GaTa_4Se_8$, npj Quantum Mater. **5**, 41 (2020).

[18] J. Maciejko, V. Chua, and G. A. Fiete, *Topological Order in a Correlated Three-Dimensional Topological Insulator*, Phys. Rev. Lett. **112**, 016404 (2014).

[19] W. Witczak-Krempa, G. Chen, Y. B. Kim, and L. Balents, *Correlated Quantum Phenomena in the Strong Spin-Orbit Regime*, Annu. Rev. Condens. Matter Phys. **5**, 57 (2014).

[20] M.-W. Yoo, J. Tornos, A. Sander, L.-F. Lin, N. Mohanta, A. Peralta, D. Sanchez-Manzano, F. Gallego, D. Haskel, J. W. Freeland *et al.*, *Large Intrinsic Anomalous Hall Effect in* $SrIrO_3$ *Induced by Magnetic Proximity Effect*, Nat. Commun. **12**, 3283 (2021).

[21] Z. Xiang, Y. Kasahara, T. Asaba, B. Lawson, C. Tinsman, L. Chen, K. Sugimoto, S. Kawaguchi, Y. Sato, G. Li, S. Yao, Y. L. Chen, F. Iga, J. Singleton, Y. Matsuda, and L. Li, *Quantum Oscillations of Electrical Resistivity in an Insulator*, Science **362**, 65 (2018).

[22] Z. Xiang, L. Chen, K.-W. Chen, C. Tinsman, Y. Sato, T. Asaba, H. Lu, Y. Kasahara, M. Jaime, F. Balakirev, F. Iga, Y. Matsuda, J. Singleton, and L. Li, *Unusual High-Field Metal in a Kondo Insulator*, Nat. Phys. **17**, 788 (2021).

[23] F. D. M. Haldane, *O(3) Nonlinear σ Model and the Topological Distinction between Integer- and Half-Integer-Spin Antiferromagnets in Two Dimensions*, Phys. Rev. Lett. **61**, 1029 (1988).

[24] C. L. Kane and E. J. Mele, Z_2 *Topological Order and the Quantum Spin Hall Effect*, Phys. Rev. Lett. **95**, 146802 (2005).

[25] C. L. Kane and E. J. Mele, *Quantum Spin Hall Effect in Graphene*, Phys. Rev. Lett. **95**, 226801 (2005).

[26] P. W. Anderson, *Antiferromagnetism. Theory of Superexchange Interaction*, Phys. Rev. **79**, 350 (1950).

[27] S. Raghu, X.-L. Qi, C. Honerkamp, and S.-C. Zhang, *Topological Mott Insulators*, Phys. Rev. Lett. **100**, 156401 (2008).

[28] J. N. Nelson, C. T. Parzyck, B. D. Faeth, J. K. Kawasaki, D. G. Schlom, and K. M. Shen, *Mott Gap Collapse in Lightly Hole-Doped* $Sr_{2-x}K_xIrO_4$, Nat. Commun. **11**, 2597 (2020).

[29] B. Xu, P. Marsik, E. Sheveleva, F. Lyzwa, A. Louat, V. Brouet, D. Munzar, and C. Bernhard, *Optical Signature of a Crossover from Mott- to Slater-Type Gap in* $Sr_2Ir_{1-x}Rh_xO_4$, Phys. Rev. Lett. **124**, 027402 (2020).

[30] J. Yang, L. Hao, D. Meyers, T. Dasa, L. Xu, L. Horak, P. Shafer, E. Arenholz, G. Fabbris, Y. Choi, D. Haskel, J. Karapetrova, J.-W. Kim, P. J. Ryan, H. Xu, C. D. Batista, M. P. M. Dean, and J. Liu, *Strain-Modulated Slater-Mott Crossover of Pseudospin-Half Square-Lattice in* $(SrIrO_3)_1/(SrTiO_3)_1$ *Superlattices*, Phys. Rev. Lett. **124**, 177601 (2020).

[31] B. Zwartsenberg, R. P. Day, E. Razzoli, M. Michiardi, N. Xu, M. Shi, J. D. Denlinger, G. Cao, S. Calder, K. Ueda, J. Bertinshaw, H. Takagi, B. J. Kim, I. S. Elfimov, and A. Damascelli, *Spin-Orbit-Controlled Metal–Insulator Transition in* Sr_2IrO_4, Nat. Phys. **16**, 290 (2020).

[32] J. P. F. LeBlanc, A. E. Antipov, F. Becca, I. W. Bulik, G. K.-L. Chan, C.-M. Chung, Y. Deng, M. Ferrero, T. M. Henderson, C. A. Jiménez-Hoyos *et al.*, *Solutions of the Two-Dimensional Hubbard Model: Benchmarks and Results from a Wide Range of Numerical Algorithms*, Phys. Rev. X **5**, 041041 (2015).

[33] L. Hao, Z. Wang, J. Yang, D. Meyers, J. Sanchez, G. Fabbris, Y. Choi, J.-W. Kim, D. Haskel, P. J. Ryan, K. Barros, J.-H. Chu, M. P. M. Dean, C. D. Batista, and J. Liu, *Anomalous Magnetoresistance due to Longitudinal Spin Fluctuations in a* $J_{\mathrm{eff}} = 1/2$ *Mott Semiconductor*, Nat. Commun. **10**, 5301 (2019).

[34] E. Manousakis, *The Spin-*$1/2$ *Heisenberg Antiferromagnet on a Square Lattice and Its Application to the Cuprous Oxides*, Rev. Mod. Phys. **63**, 1 (1991).

[35] G. Jackeli and G. Khaliullin, *Mott Insulators in the Strong Spin-Orbit Coupling Limit: From Heisenberg to a Quantum Compass and Kitaev Models*, Phys. Rev. Lett. **102**, 017205 (2009).

[36] B. J. Kim, H. Ohsumi, T. Komesu, S. Sakai, T. Morita, H. Takagi, and T. Arima, *Phase-Sensitive Observation of a Spin-Orbital Mott State in* Sr_2IrO_4, Science **323**, 1329 (2009).

[37] J. G. Rau, E. K.-H. Lee, and H.-Y. Kee, *Spin-Orbit Physics Giving Rise to Novel Phases in Correlated Systems: Iridates and Related Materials*, Annu. Rev. Condens. Matter Phys. **7**, 195 (2016).

[38] R. Schaffer, E. K. H. Lee, B. J. Yang, and Y. B. Kim, *Recent Progress on Correlated Electron Systems with Strong Spin-Orbit Coupling*, Rep. Prog. Phys. **79**, 094504 (2016).

[39] J. Bertinshaw, Y. K. Kim, G. Khaliullin, and B. J. Kim, *Square Lattice Iridates*, Annu. Rev. Condens. Matter Phys. **10**, 315 (2019).

[40] B. J. Kim, H. Jin, S. J. Moon, J. Y. Kim, B. G. Park, C. S. Leem, J. Yu, T. W. Noh, C. Kim, S. J. Oh, J. H. Park, V. Durairaj, G. Cao, and E. Rotenberg, *Novel* $J_{\mathrm{eff}} = 1/2$ *Mott State Induced by Relativistic Spin-Orbit Coupling in* Sr_2IrO_4, Phys. Rev. Lett. **101**, 076402 (2008).

[41] G. Cao and P. Schlottmann, *The Challenge of Spin–Orbit-Tuned Ground States in Iridates: A Key Issues Review*, Rep. Prog. Phys. **81**, 042502 (2018).

[42] H. Watanabe, T. Shirakawa, and S. Yunoki, *Microscopic Study of a Spin-Orbit-Induced Mott Insulator in Ir Oxides*, Phys. Rev. Lett. **105**, 216410 (2010).

[43] F. Wang and T. Senthil, *Twisted Hubbard Model for* Sr_2IrO_4*: Magnetism and Possible High Temperature Superconductivity*, Phys. Rev. Lett. **106**, 136402 (2011).

[44] J.-M. Carter, V. Shankar V., and H.-Y. Kee, *Theory of Metal-Insulator Transition in the Family of Perovskite Iridium Oxides*, Phys. Rev. B **88**, 035111 (2013).

[45] Y. Chen and H.-Y. Kee, *Topological Phases in Iridium Oxide Superlattices: Quantized Anomalous Charge or Valley Hall Insulators*, Phys. Rev. B **90**, 195145 (2014).

[46] L. Shekhtman, O. Entin-Wohlman, and A. Aharony, *Moriya's Anisotropic Superexchange Interaction, Frustration, and Dzyaloshinsky's Weak Ferromagnetism*, Phys. Rev. Lett. **69**, 836 (1992).

[47] E. Fradkin, *Field Theories of Condensed Matter Physics* (Cambridge University Press, Cambridge, England, 2013).

[48] L. Shekhtman, A. Aharony, and O. Entin-Wohlman, *Bond-Dependent Symmetric and Antisymmetric Superexchange Interactions in* La_2CuO_4, Phys. Rev. B **47**, 174 (1993).

[49] S. J. Moon, H. Jin, K. W. Kim, W. S. Choi, Y. S. Lee, J. Yu, G. Cao, A. Sumi, H. Funakubo, C. Bernhard, and T. W. Noh, *Dimensionality-Controlled Insulator-Metal Transition and Correlated Metallic State in 5d Transition Metal Oxides* $Sr_{n+1}Ir_nO_{3n+1}$ *($n = 1, 2$, and ∞)*, Phys. Rev. Lett. **101**, 226402 (2008).

[50] S. Y. Kim, C. H. Kim, L. J. Sandilands, C. H. Sohn, J. Matsuno, H. Takagi, K. W. Kim, Y. S. Lee, S. J. Moon, and T. W. Noh, *Manipulation of Electronic Structure via Alteration of Local Orbital Environment in* $[(SrIrO_3)_m, (SrTiO_3)]$ *($m = 1, 2$, and ∞) Superlattices*, Phys. Rev. B **94**, 245113 (2016).

[51] J. Matsuno, K. Ihara, S. Yamamura, H. Wadati, K. Ishii, V. V. Shankar, H. Y. Kee, and H. Takagi, *Engineering a Spin-Orbital Magnetic Insulator by Tailoring Superlattices*, Phys. Rev. Lett. **114**, 247209 (2015).

[52] L. Hao, D. Meyers, C. Frederick, G. Fabbris, J. Yang, N. Traynor, L. Horak, D. Kriegner, Y. Choi, J.-W. Kim, D. Haskel, P. J. Ryan, M. P. M. Dean, and J. Liu, *Two-Dimensional* $J_{\mathrm{eff}} = 1/2$ *Antiferromagnetic Insulator Unraveled from Interlayer Exchange Coupling in Artificial Perovskite Iridate Superlattices*, Phys. Rev. Lett. **119**, 027204 (2017).

[53] See Supplemental Material at http://link.aps.org/supplemental/10.1103/PhysRevX.12.031015 for additional information on synchrotron-XRD, STEM, XAS, RIXS measurements, and theoretical analysis.

[54] A. M. Glazer, *Simple Ways of Determining Perovskite Structures*, Acta Crystallogr. Sect. A **31**, 756 (1975).

[55] T. R. Dasa, L. Hao, J. Liu, and H. Xu, *Designing Iridate-Based Superlattice with Large Magnetoelectric Coupling*, J. Mater. Chem. C **7**, 13294 (2019).

[56] M. Oshikawa and I. Affleck, *Field-Induced Gap in* $S = 1/2$ *Antiferromagnetic Chains*, Phys. Rev. Lett. **79**, 2883 (1997).

[57] M. Lee, Y. Onose, Y. Tokura, and N. P. Ong, *Hidden Constant in the Anomalous Hall Effect of High-Purity Magnet MnSi*, Phys. Rev. B **75**, 172403 (2007).

[58] J. Matsuno, N. Ogawa, K. Yasuda, F. Kagawa, W. Koshibae, N. Nagaosa, Y. Tokura, and M. Kawasaki, *Interface-Driven Topological Hall Effect in* $SrRuO_3 - SrIrO_3$ *Bilayer*, Sci. Adv. **2**, e1600304 (2016).

[59] J. Nichols, X. Gao, S. Lee, T. L. Meyer, J. W. Freeland, V. Lauter, D. Yi, J. Liu, D. Haskel, J. R. Petrie, E.-J. Guo, A. Herklotz, D. Lee, T. Z. Ward, G. Eres, M. R. Fitzsimmons, and H. N. Lee, *Emerging Magnetism and Anomalous Hall Effect in Iridate–Manganite Heterostructures*, Nat. Commun. **7**, 12721 (2016).

[60] D. Yi, J. Liu, S. L. Hsu, L. P. Zhang, Y. Choi, J. W. Kim, Z. H. Chen, J. D. Clarkson, C. R. Serrao, E. Arenholz, P. J. Ryan, H. X. Xu, R. J. Birgeneau, and R. Ramesh, *Atomic-Scale Control of Magnetic Anisotropy via Novel Spin-Orbit Coupling Effect in* $La_{2/3}Sr_{1/3}MnO_3/SrIrO_3$ *Superlattices*, Proc. Natl. Acad. Sci. U.S.A. **113**, 6397 (2016).

[61] D. Yi, Y. Wang, O. M. J. van't Erve, L. Xu, H. Yuan, M. J. Veit, P. P. Balakrishnan, Y. Choi, A. T. N'Diaye, P. Shafer, E. Arenholz, A. Grutter, H. Xu, P. Yu, B. T. Jonker, and Y. Suzuki, *Emergent Electric Field Control of Phase Transformation in Oxide Superlattices*, Nat. Commun. **11**, 902 (2020).

[62] A. K. Jaiswal, D. Wang, V. Wollersen, R. Schneider, M. L. Tacon, and D. Fuchs, *Direct Observation of Strong Anomalous Hall Effect and Proximity-Induced Ferromagnetic State in* $SrIrO_3$, Adv. Mater. **34**, 2109163 (2022).

[63] K. Ohgushi, S. Murakami, and N. Nagaosa, *Spin Anisotropy and Quantum Hall Effect in the Kagome Lattice: Chiral Spin State Based on a Ferromagnet*, Phys. Rev. B **62**, R6065 (2000).

[64] D. Coffey, T. M. Rice, and F. C. Zhang, *Dzyaloshinskii-Moriya Interaction in the Cuprates*, Phys. Rev. B **44**, 10112 (1991).

[65] D. Schattschneider, *The Plane Symmetry Groups: Their Recognition and Notation*, Am. Math. Mon. **85**, 439 (1978).

[66] T. Moriya, *Anisotropic Superexchange Interaction and Weak Ferromagnetism*, Phys. Rev. **120**, 91 (1960).

[67] T. Moriya, *New Mechanism of Anisotropic Superexchange Interaction*, Phys. Rev. Lett. **4**, 228 (1960).

[68] I. Dzyaloshinsky, *A Thermodynamic Theory of "Weak" Ferromagnetism of Antiferromagnetics*, J. Phys. Chem. Solids **4**, 241 (1958).

[69] H. Kuwahara, R. Kawasaki, Y. Hirobe, S. Kodama, and A. Kakishima, *Anomalous Hall Effect and Magnetoresistance in* $Nd_{1-x}Sr_xMnO_3$ *Single Crystals*, J. Appl. Phys. **93**, 7367 (2003).

[70] L. Klein, J. R. Reiner, T. H. Geballe, M. R. Beasley, and A. Kapitulnik, *Extraordinary Hall Effect in* $SrRuO_3$, Phys. Rev. B **61**, R7842 (2000).

[71] D. Pincini, J. G. Vale, C. Donnerer, A. de la Torre, E. C. Hunter, R. Perry, M. Moretti Sala, F. Baumberger, and D. F. McMorrow, *Anisotropic Exchange and Spin-Wave Damping in Pure and Electron-Doped* Sr_2IrO_4, Phys. Rev. B **96**, 075162 (2017).

[72] H. Gretarsson, N. H. Sung, J. Porras, J. Bertinshaw, C. Dietl, J. A. N. Bruin, A. F. Bangura, Y. K. Kim, R. Dinnebier, J. Kim, A. Al-Zein, M. Moretti Sala, M. Krisch, M. Le Tacon, B. Keimer, and B. J. Kim, *Persistent Paramagnons Deep in the Metallic Phase of* $Sr_{2-x}La_xIrO_4$, Phys. Rev. Lett. **117**, 107001 (2016).

[73] X. Liu, M. P. M. Dean, Z. Y. Meng, M. H. Upton, T. Qi, T. Gog, Y. Cao, J. Q. Lin, D. Meyers, H. Ding, G. Cao, and J. P. Hill, *Anisotropic Softening of Magnetic Excitations in Lightly Electron-Doped* Sr_2IrO_4, Phys. Rev. B **93**, 241102(R) (2016).

[74] S. Calder, D. M. Pajerowski, M. B. Stone, and A. F. May, *Spin-Gap and Two-Dimensional Magnetic Excitations in* Sr_2IrO_4, Phys. Rev. B **98**, 220402 (2018).

[75] A. Lupascu, J. P. Clancy, H. Gretarsson, Z. Nie, J. Nichols, J. Terzic, G. Cao, S. S. A. Seo, Z. Islam, M. H. Upton, J. Kim, D. Casa, T. Gog, A. H. Said, V. M. Katukuri, H. Stoll, L. Hozoi, J. van den Brink, and Y.-J. Kim, *Tuning Magnetic Coupling in* Sr_2IrO_4 *Thin Films with Epitaxial Strain*, Phys. Rev. Lett. **112**, 147201 (2014).

[76] D. Meyers, Y. Cao, G. Fabbris, N. J. Robinson, L. Hao, C. Frederick, N. Traynor, J. Yang, J. Lin, M. H. Upton *et al.*, *Magnetism in Iridate Heterostructures Leveraged by Structural Distortions*, Sci. Rep. **9**, 4263 (2019).

[77] D. Meyers, K. Nakatsukasa, S. Mu, L. Hao, J. Yang, Y. Cao, G. Fabbris, H. Miao, J. Pelliciari, D. McNally *et al.*, *Decoupling Carrier Concentration and Electron-Phonon Coupling in Oxide Heterostructures Observed with Resonant Inelastic X-Ray Scattering*, Phys. Rev. Lett. **121**, 236802 (2018).

[78] J. Kim, D. Casa, M. H. Upton, T. Gog, Y.-J. Kim, J. F. Mitchell, M. van Veenendaal, M. Daghofer, J. van den Brink, G. Khaliullin, and B. J. Kim, *Magnetic Excitation Spectra of* Sr_2IrO_4 *Probed by Resonant Inelastic X-Ray Scattering: Establishing Links to Cuprate Superconductors*, Phys. Rev. Lett. **108**, 177003 (2012).

[79] J. Kim, M. Daghofer, A. H. Said, T. Gog, J. van den Brink, G. Khaliullin, and B. J. Kim, *Excitonic Quasiparticles in a Spin–Orbit Mott Insulator*, Nat. Commun. **5**, 4453 (2014).

[80] H. Suwa (unpublished).

[81] H. Suwa, S.-S. Zhang, and C. D. Batista, *Exciton Condensation in Bilayer Spin-Orbit Insulator*, Phys. Rev. Research **3**, 013224 (2021).

[82] D. G. Mazzone, Y. Shen, H. Suwa, G. Fabbris, J. Yang, S. S. Zhang, H. Miao, J. Sears, K. Jia, Y. G. Shi, M. H. Upton, D. M. Casa, X. Liu, J. Liu, C. D. Batista, and M. P. M. Dean, *Antiferromagnetic Excitonic Insulator State in* $Sr_3Ir_2O_7$, Nat. Commun. **13**, 913 (2022).

[83] J. Kim, A. H. Said, D. Casa, M. H. Upton, T. Gog, M. Daghofer, G. Jackeli, J. van den Brink, G. Khaliullin, and B. J. Kim, *Large Spin-Wave Energy Gap in the Bilayer Iridate* $Sr_3Ir_2O_7$*: Evidence for Enhanced Dipolar Interactions Near the Mott Metal-Insulator Transition*, Phys. Rev. Lett. **109**, 157402 (2012).

[84] J. W. Kim, Y. Choi, J. Kim, J. F. Mitchell, G. Jackeli, M. Daghofer, J. van den Brink, G. Khaliullin, and B. J. Kim, *Dimensionality Driven Spin-Flop Transition in Layered Iridates*, Phys. Rev. Lett. **109**, 037204 (2012).

[85] T. Hogan, L. Bjaalie, L. Zhao, C. Belvin, X. Wang, C. G. Van de Walle, D. Hsieh, and S. D. Wilson, *Structural Investigation of the Bilayer Iridate* $Sr_3Ir_2O_7$, Phys. Rev. B **93**, 134110 (2016).

[86] X. Liu, H.-C. Hsu, and C.-X. Liu, *In-Plane Magnetization-Induced Quantum Anomalous Hall Effect*, Phys. Rev. Lett. **111**, 086802 (2013).